



## ORIGINAL RESEARCH

# Npac Is A Co-factor of Histone H3K36me3 and Regulates Transcriptional Elongation in Mouse Embryonic Stem Cells



Sue Yu<sup>1,#</sup>, Jia Li<sup>2,#</sup>, Guanxu Ji<sup>3</sup>, Zhen Long Ng<sup>1</sup>, Jiamin Siew<sup>1</sup>,  
Wan Ning Lo<sup>1</sup>, Ying Ye<sup>4</sup>, Yuan Yuan Chew<sup>1</sup>, Yun Chau Long<sup>1</sup>,  
Wensheng Zhang<sup>4</sup>, Ernesto Guccione<sup>5</sup>, Yui Han Loh<sup>5</sup>, Zhi-Hong Jiang<sup>3</sup>,  
Henry Yang<sup>2,\*</sup>, Qiang Wu<sup>1,3,\*</sup>

<sup>1</sup> Department of Biochemistry, Yong Loo Lin School of Medicine, National University of Singapore, Singapore 117597, Singapore

<sup>2</sup> Cancer Science Institute of Singapore, Centre for Translational Medicine, Singapore 117599, Singapore

<sup>3</sup> The State Key Laboratory of Quality Research in Chinese Medicine, Macau University of Science and Technology, Macau Special Administrative Region 999078, China

<sup>4</sup> Cam-Su Genomic Resource Center, Soochow University, Suzhou 215123, China

<sup>5</sup> Institute of Molecular and Cell Biology, Singapore 138673, Singapore

Received 19 October 2019; revised 16 July 2020; accepted 15 August 2020

Available online 4 March 2021

Handled by Jiang Liu

## KEYWORDS

Npac;  
Pluripotency;  
Reprogramming;  
Histone H3K36me3;  
Transcriptional elongation

**Abstract** Chromatin modification contributes to **pluripotency** maintenance in embryonic stem cells (ESCs). However, the related mechanisms remain obscure. Here, we show that **Npac**, a “reader” of histone H3 lysine 36 trimethylation (H3K36me3), is required to maintain mouse ESC (mESC) pluripotency since knockdown of *Npac* causes mESC differentiation. Depletion of *Npac* in mouse embryonic fibroblasts (MEFs) inhibits **reprogramming** efficiency. Furthermore, our chromatin immunoprecipitation followed by sequencing (ChIP-seq) results of *Npac* reveal that *Npac* co-localizes with **histone H3K36me3** in gene bodies of actively transcribed genes in mESCs. Interestingly, we find that *Npac* interacts with positive transcription elongation factor b (p-TEFb), Ser2-phosphorylated RNA Pol II (RNA Pol II Ser2P), and Ser5-phosphorylated RNA Pol II (RNA Pol II Ser5P). Furthermore, depletion of *Npac* disrupts **transcriptional**

\* Corresponding authors.

E-mail: [csiyangh@nus.edu.sg](mailto:csiyangh@nus.edu.sg) (Yang H), [qw@must.edu.mo](mailto:qw@must.edu.mo) (Wu Q).

# Equal contribution.

Peer review under responsibility of Beijing Institute of Genomics, Chinese Academy of Sciences / China National Center for Bioinformation and Genetics Society of China.

<https://doi.org/10.1016/j.gpb.2020.08.004>

1672-0229 © 2022 The Authors. Published by Elsevier B.V. and Science Press on behalf of Beijing Institute of Genomics, Chinese Academy of Sciences / China National Center for Bioinformation and Genetics Society of China.

This is an open access article under the CC BY-NC-ND license (<http://creativecommons.org/licenses/by-nc-nd/4.0/>).

**elongation** of the pluripotency genes *Nanog* and *Rif1*. Taken together, we propose that *Npac* is essential for the transcriptional elongation of pluripotency genes by recruiting p-TEFb and interacting with RNA Pol II Ser2P and Ser5P.

## Introduction

Embryonic stem cells (ESCs) derived from the inner cell mass of the early embryo are characterized by self-renewal and pluripotency (*i.e.*, the ability to differentiate into many different cell types) [1,2]. Since ESCs can be cultured indefinitely *in vitro*, they are a promising resource for regenerative therapy. In particular, ESCs show potential for treating degenerative diseases such as diabetes and Parkinson's disease [3,4]. Moreover, induced pluripotent stem cells (iPSCs) show enormous potential for the application and progress in gene therapy and regenerative medicine [5–8]. Therefore, enhanced understanding of the molecular mechanisms regulating ESC identity would be of great value toward developing ESC- and iPSC-based therapies.

Transcription factors Oct4 (encoded by the *Pou5f1* gene), Sox2, and Nanog constitute the core transcriptional network that activates genes that promote pluripotency and self-renewal and inhibits genes that promote differentiation [9–12]. Yamanaka's discovery that the combination of transcription factors Oct4, Klf4, Sox2, and c-Myc (OKSM) is sufficient to reprogram terminally differentiated cells to pluripotent stem cells has further proved the importance of those core transcription factors [7]. Aside from these, many other transcription factors are essential for pluripotency [13–16].

Besides transcription factors, chromatin regulators also contribute to mouse ESC (mESC) pluripotency through providing the necessary environment for proper gene expression [17]. Recently, a handful of chromatin regulators that are critical for ESC pluripotency have been characterized. ESCs contain structurally relaxed and transcriptionally permissive chromatin that allows for epigenetic remodeling [18]. However, factors that modify the epigenetic configuration are not completely known. Lysine-trimethylation modifications at histone H3 are the most stable epigenetic marks on histones. ESCs are featured by a higher level of histone H3 lysine 4 trimethylation (H3K4me3), which is generally correlated with gene activation [19]. Conversely, H3K27me3 and H3K9me3 are related to gene silencing and heterochromatin in ESCs [20]. However, few studies have examined the regulation of histone H3K36me3 in ESCs [21,22]. Histone H3K36me3 marks active genes, preferentially occupies exons and introns (gene bodies) [23], and is considered as a mark of transcriptional elongation. Recently, a large-scale methyl lysine interactome study discovered proteins that bind to specific histone marks [24]. Interestingly, all proteins that bind to histone H3K36me3 have a common proline-tryptophan-tryptophan-proline (PWWP) domain. This and other studies [25–27] suggest the essential role of the PWWP domain in binding to histone H3K36me3.

*Npac* (also known as NP60 and Gylr1) containing a PWWP domain is one of the proteins that can bind to histone H3K36me3 [24]. A chromatin immunoprecipitation followed by sequencing (ChIP-seq) analysis on human chromosome 22 revealed that both histone H3K36me3 and *Npac* are exclusively localized in gene bodies [24], suggesting that *Npac*

may function in transcriptional elongation. Additionally, *Npac* is a co-factor of lysine-specific demethylase 2 (LSD2) which mediates histone H3K4 demethylation [28–30]. These findings suggest that *Npac* regulates gene expression through interacting with specific histone modifications. However, how *Npac* plays its roles is largely unknown.

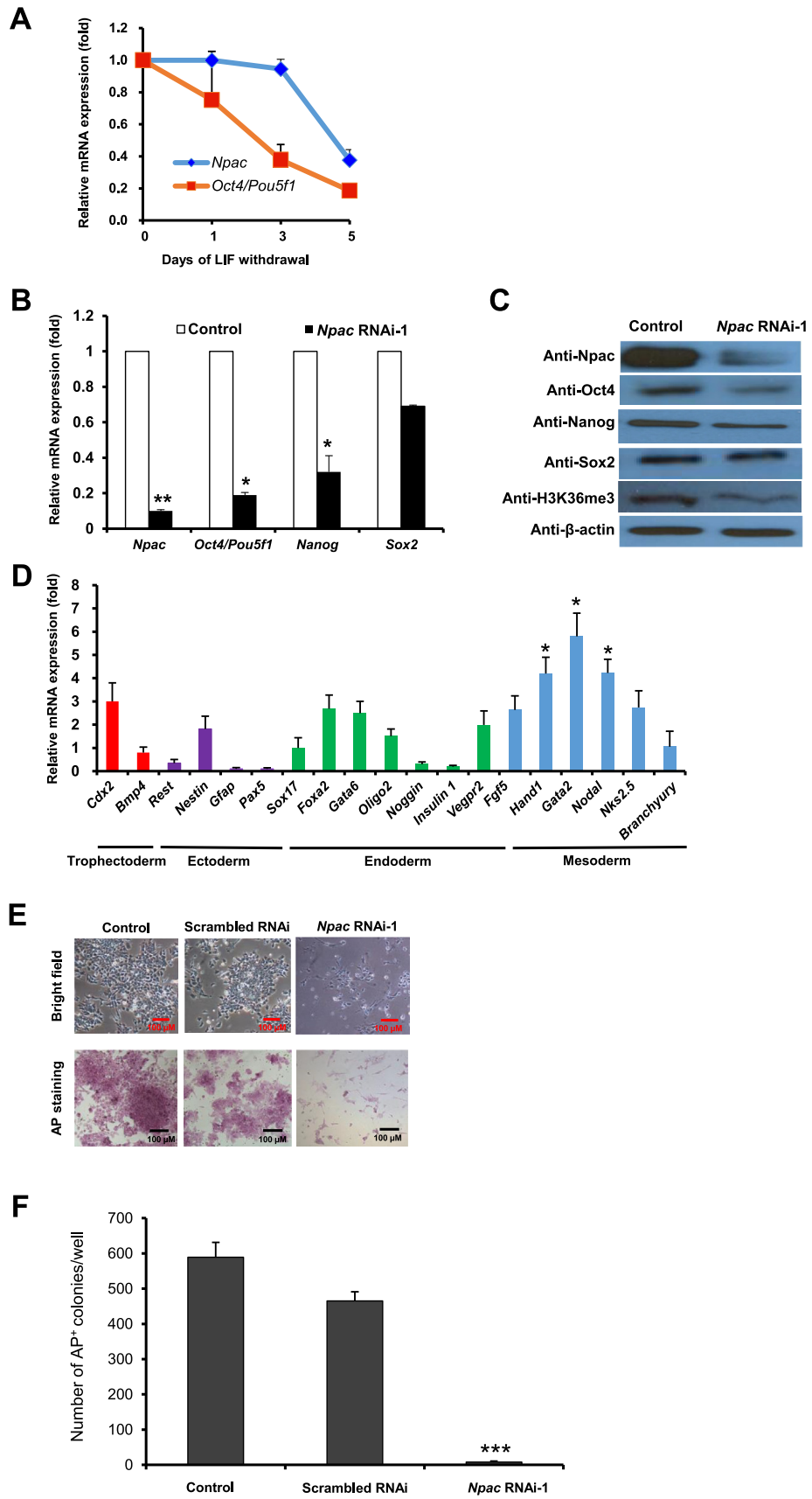
In this study, we found that *Npac* is required to maintain mESC pluripotency. Depletion of *Npac* leads to mESC differentiation with loss of pluripotency. Depletion of *Npac* also reduces the reprogramming efficiency of mouse embryonic fibroblasts (MEFs). We observed that *Npac* positively regulates pluripotency genes such as *Oct4/Pou5f1* and *Nanog*. *Npac* may prevent mESC differentiation by repressing the MAPK/ERK pathway. Furthermore, ChIP-seq experiments showed that *Npac* co-localizes with histone H3K36me3 in the body of genes which are actively transcribed in mESCs. *Npac* interacts with RNA Pol II (including Ser2- and Ser5-phosphorylated RNA Pol II; RNA Pol II Ser2P and Ser5P) and positive transcription elongation factor b (p-TEFb), and *Npac* depletion causes transcriptional elongation defects of *Nanog* and *Rif1*. Together, these results establish that *Npac* maintains mESC pluripotency and regulates transcriptional elongation in mESCs.

## Results

### *Npac* is required for maintenance of mESC pluripotency

To test whether *Npac* is associated with ESC pluripotency, we induced mESCs to differentiate by using ES medium without leukemia inhibitory factor (LIF). We observed that the *Npac* mRNA level was decreased during differentiation, dropping to around 40% at 5 days after LIF removal (Figure 1A).

Next, we depleted *Npac* by RNAi to determine the role of *Npac* in ESC pluripotency. Transfection of mESCs with shRNA plasmids (*Npac* RNAi-1 or RNAi-2) targeting *Npac* significantly reduced the level of *Npac* mRNA (Figure 1B, Figure S1A). We observed that transfection with *Npac* RNAi-1 significantly reduced the mRNA levels of ESC pluripotency genes *Oct4/Pou5f1* and *Nanog* (Figure 1B). Additionally, the protein levels of Oct4 and Nanog, as well as the H3K36me3 level, were reduced in *Npac* RNAi-1 transfected ESCs (Figure 1C). The mRNA expression levels of *Oct4/Pou5f1* and *Nanog* were also significantly down-regulated in *Npac* RNAi-2 transfected ESCs (Figure S1A). The reduction of Oct4 and Nanog upon *Npac* knockdown (KD) suggested that *Npac* depletion may cause loss of ESC pluripotency, since Oct4 and Nanog are master regulators required to maintain ESC pluripotency [13–15,31]. This was further supported by the evidence that certain lineage marker genes were up-regulated upon *Npac* depletion: the trophoblast marker *Cdx2* showed a 2-fold increase; the endoderm markers *Foxa2*, *Gata6*, and *Vegfr2* displayed 1.7-, 1.5-, and 1-fold increase, respectively; the mesoderm markers *Nodal*, *Hand1*, and *Gata2* increased by 3.2, 3.2, and 4.8 folds, respectively (Figure 1D). Moreover, *Npac* RNAi-1 transfected ESCs



showed morphological differentiation and weaker alkaline phosphatase (AP) activity compared to control cells transfected with empty vector, while scrambled RNAi transfected cells appeared to have an AP activity similar to the control (Figure 1E and F), further indicating that *Npac*-depleted cells underwent differentiation.

To ensure that the *Npac* RNAi was specific, we performed a *Npac* RNAi rescue experiment. To construct the *Npac* RNAi-resistant plasmid, specific primers were designed, and the plasmid with the full-length *Npac* cDNA inserted in the pCAG-Neo vector was used as the template. We transfected mouse E14 ESCs with the control (empty vector) or *Npac* RNAi-1 plasmid and selected with puromycin. We then transfected the cells with the *Npac* RNAi-resistant plasmid for RNAi rescue. The cells were selected with neomycin for 3 days, followed by AP staining. We observed sustained expression levels of the pluripotency genes *Oct4/Pou5f1*, *Nanog*, and *Sox2* and more AP-positive cells after the rescue treatment (named *Npac* RNAi-immune OE) than the control cells, showing that *Npac* RNAi-immune OE cells were resistant to *Npac* RNAi (Figure S1B and C). We also observed that the changes in AP staining and pluripotency gene expression could only be partially rescued. This is likely due to ESC differentiation caused by *Npac* RNAi before we transfected the *Npac* RNAi-resistant plasmid into the cells.

To further confirm the important role of *Npac* in pluripotency maintenance, we generated embryoid bodies (EBs) from *Npac*-depleted cells and control cells transfected with empty vector. We then cultured the EBs without LIF in low-attachment dishes for 14 days. EBs partially mimic *in vivo* embryonic development [32]. We then performed AP staining and found that EBs generated from control cells and *Npac* RNAi-1 transfected cells both lost pluripotency, while *Npac* RNAi-1-derived EBs were much smaller than the control group. These results suggest that *Npac*-depleted EBs grew more slowly than control EBs (Figure S1D). We also performed qRT-PCR to determine the expression levels of lineage markers in EBs generated from control cells and *Npac* RNAi-1 transfected cells (Figure S1E). We found that the *Npac* expression level in *Npac*-depleted EBs was lower than that in control EBs. The expression levels of several mesoderm markers (*Hand1*, *Gata2*, and *Nkx2.5*) were much higher in *Npac*-depleted EBs than those in control EBs. In addition, endoderm markers (*Sox17*, *Foxa2*, and *Vegpr2*) showed higher expression levels in *Npac*-depleted EBs than in control EBs. These results suggest that the depletion of *Npac* may drive ESCs to differen-

tiate into endoderm and mesoderm lineages, which is consistent with the result of *Npac* KD in ESCs shown in Figure 1D.

Having seen the effect of *Npac* depletion, we next examined whether overexpression (OE) of *Npac* affects ESC pluripotency and differentiation. To this end, we performed EB formation assay using *Npac*-OE cells. After EB induction, EBs at day 7 and day 14 (which mimic early and late development respectively) were collected. We found that *Npac* was expressed at higher levels in EBs at day 7 (Figure S1F) and day 14 (Figure S1G) in *Npac*-OE EBs. Interestingly, the expression levels of *Oct4* and *Nanog* in *Npac*-OE EBs were about 2 folds that in control EBs, suggesting that pluripotency genes were sustained longer in *Npac*-OE EBs. Also, we found that the size of *Npac*-OE EBs was larger than that of control group, suggesting that *Npac* OE may promote EBs to grow faster than in the control group (Figure S1H).

Based on these results, we conclude that *Npac* is required to maintain ESC pluripotency. On the one hand, *Npac* depletion represses pluripotency genes and activates lineage marker genes. On the other hand, the expression of pluripotency genes is maintained upon *Npac* OE in differentiating ESCs.

### Reprogramming efficiency of MEFs to iPSCs is reduced upon *Npac* depletion

Having seen the essential role of *Npac* in mESC pluripotency, we next tested its role in reprogramming of somatic cells. *Pou5f1-GFP* MEFs were used to facilitate the identification of putative iPSC colonies based on GFP expression [33]. When MEFs were infected with OKSM along with *Npac*-KD virus (OKSM + *Npac*-KD), the *Npac* relative expression decreased to about 29% of the control infected with OKSM only (Figure 2A). We found that the number of GFP<sup>+</sup> colonies produced by OKSM + *Npac*-KD was 2.5 folds less than the control 14 days after infection (Figure 2B). We also confirmed this by checking the iPSC colonies using AP staining (Figure 2C and D). In addition, we performed immunostaining to examine whether the iPSCs generated by OKSM + *Npac*-KD were pluripotent. We found that these iPSCs expressed endogenous *Oct4* and *Nanog*, indicating that they were ESC-like (Figure 2E). Furthermore, we generated EBs from GFP<sup>+</sup> iPSCs, which were induced by OKSM + *Npac*-KD. Our immunostaining results showed that these iPSCs could express lineage markers of endoderm (*Nestin*), mesoderm (*SMA*), and ectoderm (*Gata4*) (Figure 2F). These results sug-

### Figure 1 *Npac* is required to maintain mESC pluripotency

**A.** The *Npac* mRNA level decreased in mESCs cultured in LIF withdrawal ESC medium. The mRNA levels of *Npac* and *Oct4/Pou5f1* were compared to those in the control cells cultured in normal ESC medium and normalized against *Actb*. **B.** The mRNA levels of the pluripotency genes *Oct4/Pou5f1*, *Sox2*, and *Nanog* were significantly decreased upon *Npac* KD. mESCs transfected with the empty pSUPER.puro vector were used as a control. **C.** *Npac* KD resulted in decreased protein levels of *Oct4*, *Sox2*, *Nanog*, and histone H3K36me3.  $\beta$ -actin served as a loading control. **D.** *Npac* KD caused up-regulation of the specific markers for endoderm and mesoderm. **E.** Representative bright field images (upper panel) of E14 cells transfected with control (empty vector), scrambled RNAi, or *Npac* RNAi-1 followed by 4 days of puromycin selection. AP staining was conducted on day 4 after transfection, and the results were shown at the bottom panel. Scale bar, 100  $\mu$ m. **F.** Quantification of AP<sup>+</sup> colonies for control (empty vector), scrambled RNAi, or *Npac* RNAi-1 transfected E14 cells. Data were shown as mean  $\pm$  SE ( $n = 3$ ). \*,  $P < 0.05$ ; \*\*,  $P < 0.01$ ; \*\*\*,  $P < 0.001$  (Student's *t*-test). ESC, embryonic stem cell; mESC, mouse ESC; LIF, leukemia inhibitory factor; KD, knockdown; H3K36me3, histone H3 lysine 36 trimethylation; AP, alkaline phosphatase.

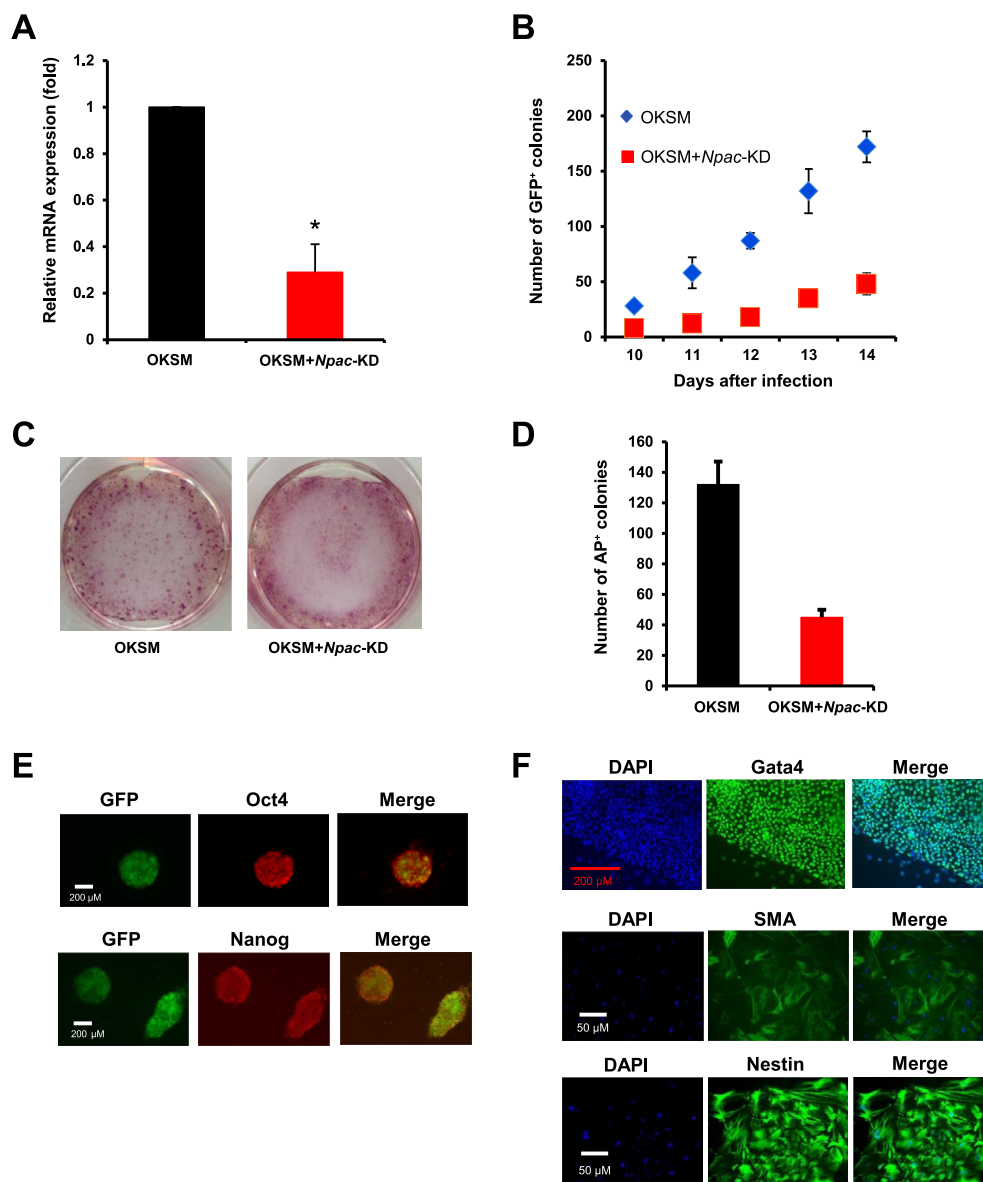


**Figure 2** Depletion of *Npac* inhibits the efficiency of reprogramming

**A.** Relative mRNA expression level of *Npac* determined by qRT-PCR in MEFs infected with OKSM alone or OKSM plus *Npac*-KD retrovirus (OKSM + *Npac*-KD). RNA was extracted from cells which were harvested 4 days after virus infection. mRNA expression levels were normalized against *Actb*. **B.** Depletion of *Npac* inhibited reprogramming efficiency. The numbers of GFP<sup>+</sup> colonies which indicate putative iPSCs were counted from day 10 to day 14 after virus infection. **C.** The iPSCs generated from OKSM + *Npac*-KD presented weaker AP activity than those from OKSM alone. **D.** Graphical representation of the AP staining results shown in (C). **E.** The iPSCs generated from OKSM + *Npac*-KD expressed Oct4 and Nanog. Immunostaining was performed with anti-Oct4 and anti-Nanog antibodies in GFP<sup>+</sup> iPSCs generated from OKSM + *Npac*-KD. **F.** EBs generated from GFP<sup>+</sup> iPSCs which were induced by OKSM + *Npac*-KD were able to express lineage markers of ectoderm (Nestin), mesoderm (SMA), and endoderm (Gata4). MEF, mouse embryonic fibroblast; OKSM, the combination of transcription factors Oct4, Klf4, Sox2, and c-Myc; EB, embryoid body.

gest that iPSCs generated by OKSM + *Npac*-KD are pluripotent. Thus, *Npac* is essential not only for the pluripotency maintenance in mESCs but also for the generation of iPSCs.

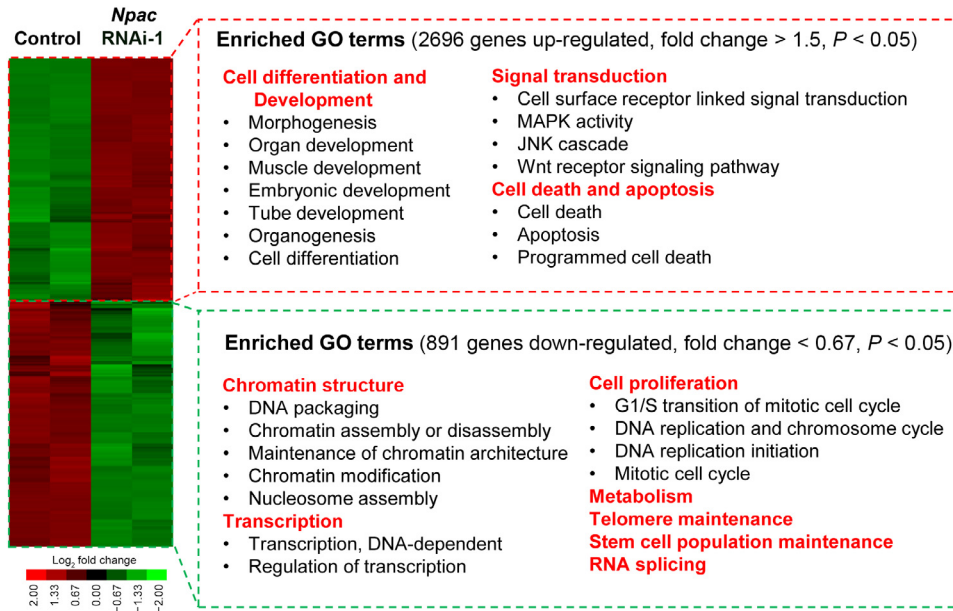
#### Depletion of *Npac* represses pluripotency genes while activating development-related genes

We next investigated how *Npac* functions in pluripotency maintenance by profiling gene expression following

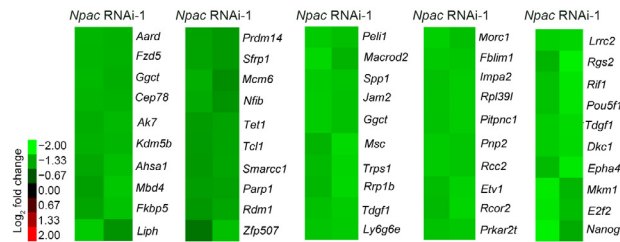
RNAi-induced *Npac* KD. Upon *Npac* depletion, the expression levels of 2696 genes were up-regulated (fold change > 1.5), while the expression levels of 891 genes were down-regulated (fold change < 0.67) (Figure 3A). We randomly chose 10 up-regulated and 9 down-regulated genes and confirmed the gene expression microarray results by qRT-PCR (Figure S2A and B).

We next carried out a Gene Ontology (GO) analysis for activated and repressed genes (Figure 3A). Full list of the

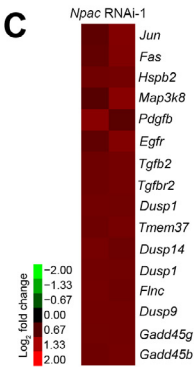
**A**



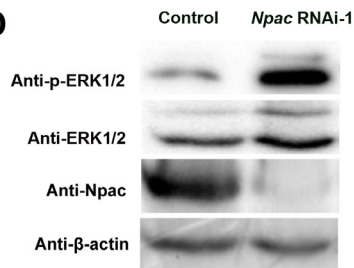
**B**



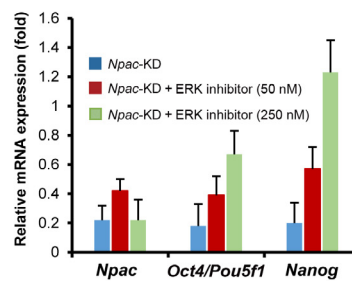
**C**



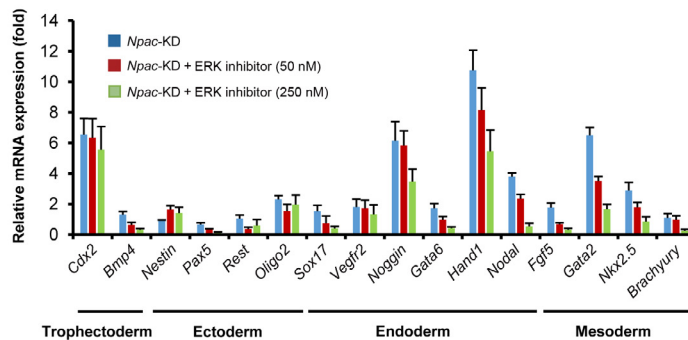
**D**



**E**



**F**



enriched terms is shown in Table S1. Among the genes down-regulated by *Npac* KD, enriched terms were related to chromosome modification, suggesting that *Npac* is required to maintain the unique chromatin structure in mESCs. Notably, we found that a majority of known pluripotency genes were down-regulated upon *Npac* depletion (Figure 3B). *Npac* could also play important roles in cell proliferation and telomere maintenance, since the GO terms related to these function groups were significantly enriched for the down-regulated genes. Among the up-regulated genes, many enriched terms were related to development (Figure 3A).

### ***Npac* regulates the MAPK/ERK pathway to influence mESC pluripotency**

Interestingly, many of the up-regulated genes upon *Npac* depletion were linked to the Wnt and MAPK signaling pathways, which are involved in mESC pluripotency (Figure 3A and C). Nichols et al. have reported that suppression of the MAPK/ERK pathway can contribute to the maintenance of the mESC ground state and pluripotency [34,35]. Also, the ERK pathway promotes mESC differentiation [36]. We found that the levels of ERK1/2 and phosphorylated ERK1/2 (p-ERK1/2) were elevated upon *Npac* depletion (Figure 3D). Thus, inhibition of the MAPK/ERK pathway by *Npac* could contribute to the effects of *Npac* on pluripotency and differentiation.

To explore the role of the MAPK pathway in *Npac* function, we tested whether inhibiting the MAPK pathway by an ERK inhibitor (PD0325901, Sigma, St. Louis, MO) could rescue the effect of *Npac* KD. We first confirmed that 50 nM/250 nM ERK inhibitor was able to block the MAPK pathway in E14 ESCs (Figure S3). We found that the ERK inhibitor did not affect *Npac* KD efficiency (Figure 3E). However, the ERK inhibitor elevated the level of *Nanog* (Figure 3E), which is in line with the previous finding that inhibition of the ERK pathway up-regulates *Nanog* in ESCs [37,38]. Furthermore, the ERK inhibitor did not rescue the down-regulation of *Oct4/Pou5f1* by *Npac* depletion (Figure 3E). Also, the ERK inhibitor reduced the expression levels of lineage markers (Figure 3F). Finally, *Npac*-depleted cells with or without the ERK inhibitor displayed similar differentiated morphology.

Taken together, our results suggest that *Npac* depletion activates the MAPK/ERK pathway, leading to mESC

differentiation. However, since blocking the MAPK/ERK pathway did not rescue the differentiation phenotype and the down-regulation of *Oct4/Pou5f1*, *Npac* likely affects pluripotency by other unknown mechanisms as well.

### ***Npac* depletion promotes apoptosis**

We also observed that many genes related to cell death and apoptosis were up-regulated when *Npac* was knocked down (Figure 4A). To evaluate the effect of *Npac* depletion on cell death, we performed propidium iodide staining and flow cytometry. Fluorescence-activated cell sorting (FACS) analysis found that the percentage of cells in the sub-G1 phase significantly increased in the *Npac*-depleted cells compared to the control group (Figure 4B and C), suggesting that there was a sub-G1 phase arrest in the cell cycle. Furthermore, Annexin V staining assay showed that apoptotic cells increased to 40.3% of the total cell population upon *Npac* depletion, compared to only 9.9% of the total cell population in the control group (Figure 4D and E). These results indicated that depletion of *Npac* caused apoptosis.

### ***Npac* is located at gene bodies and co-occupies genomic sites of histone H3K36me3**

*Oct4* and *Nanog* are master regulators in the pluripotency transcriptional network [13]. Since depletion of *Npac* down-regulates *Oct4/Pou5f1* and *Nanog*, we tested whether *Npac* is located at *Oct4/Pou5f1* and *Nanog* promoters using chromatin immunoprecipitation (ChIP). Interestingly, we found enrichment of *Npac* in the introns and exons (here defined as the gene body) of *Nanog* but not in the promoter (Figure 5A and B). Also, we did not observe any enrichment of *Npac* within the promoter of *Oct4/Pou5f1* (Figure S4). Similarly, we also found enrichment of *Npac* in the gene bodies of other pluripotent genes such as *Tcf15*, *Prdm14*, and *Tcl1* (Figure 5C).

To determine the genome-wide distribution of *Npac* in ESCs, we conducted a ChIP-seq experiment using anti-*Npac* antibody. We identified 12,414 potential genomic binding sites of *Npac*, where 2416 genes were mapped. Specifically, 57.24% of these binding sites were located within gene bodies. Additionally, 41.95% of the sites were within transcription termination sites (TTSs), followed by 0.66% and 0.15% mapped to intergenic regions and transcription start sites (TSSs),

### **Figure 3 Changes of global gene expression upon *Npac* depletion in mESCs**

**A.** Microarray heatmap generated from the relative gene expression levels. Relative highly expressed genes were shown in red and lowly expressed genes in green. *Npac* was knocked down in E14 cells and selected for 96 h. Then whole-genome cDNA microarray hybridization was performed. Duplicates were chosen to ensure the reproducibility of results. GO analysis was performed relating to “biological process” for the up- or down-regulated genes, respectively. The enriched terms were classified into several function groups and listed in the figure. **B.** Heatmap of the down-regulated pluripotency genes upon *Npac* KD in mESCs. Genes were selected according to their known functions in pluripotency. Each selected gene was taken as individual tiles from the thumbnail-dendrogram duplicates. **C.** Heatmap of the up-regulated MAPK pathway-related genes upon *Npac* KD in mESCs. Genes were selected according to their known functions in the MAPK pathway. **D.** The protein levels of p-ERK1/2 and ERK1/2 were elevated in *Npac*-depleted cells as compared to the control (empty vector) cells.  $\beta$ -actin served as a loading control. **E.** ERK inhibitor (PD0325901, Sigma) triggered elevated expression of *Nanog* but did not rescue the down-regulated expression of *Oct4* upon *Npac* KD. **F.** ERK inhibitor slightly brought down the up-regulated lineage markers in *Npac*-KD cells. GO, Gene Ontology; p-ERK1/2, phosphorylated ERK1/2.

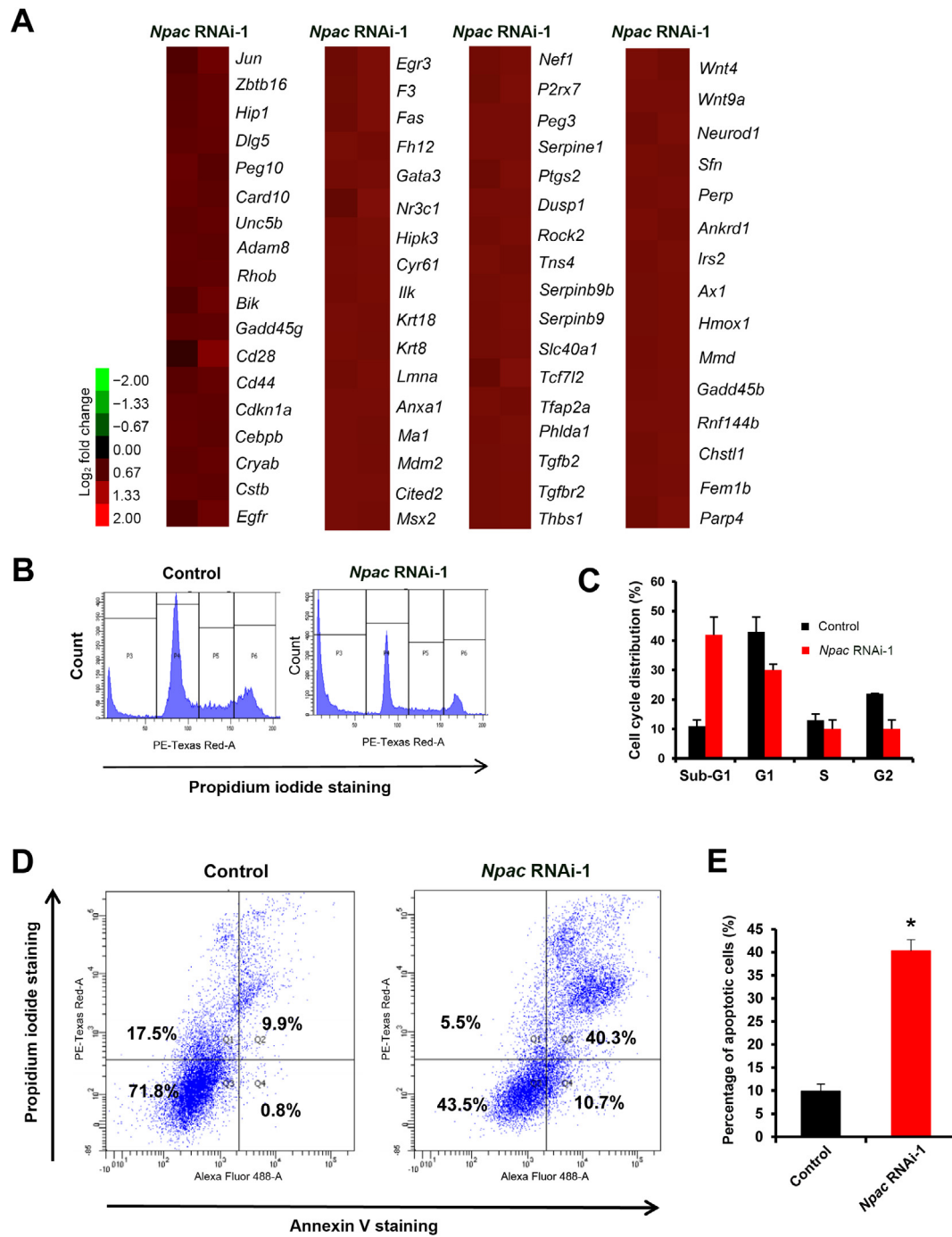
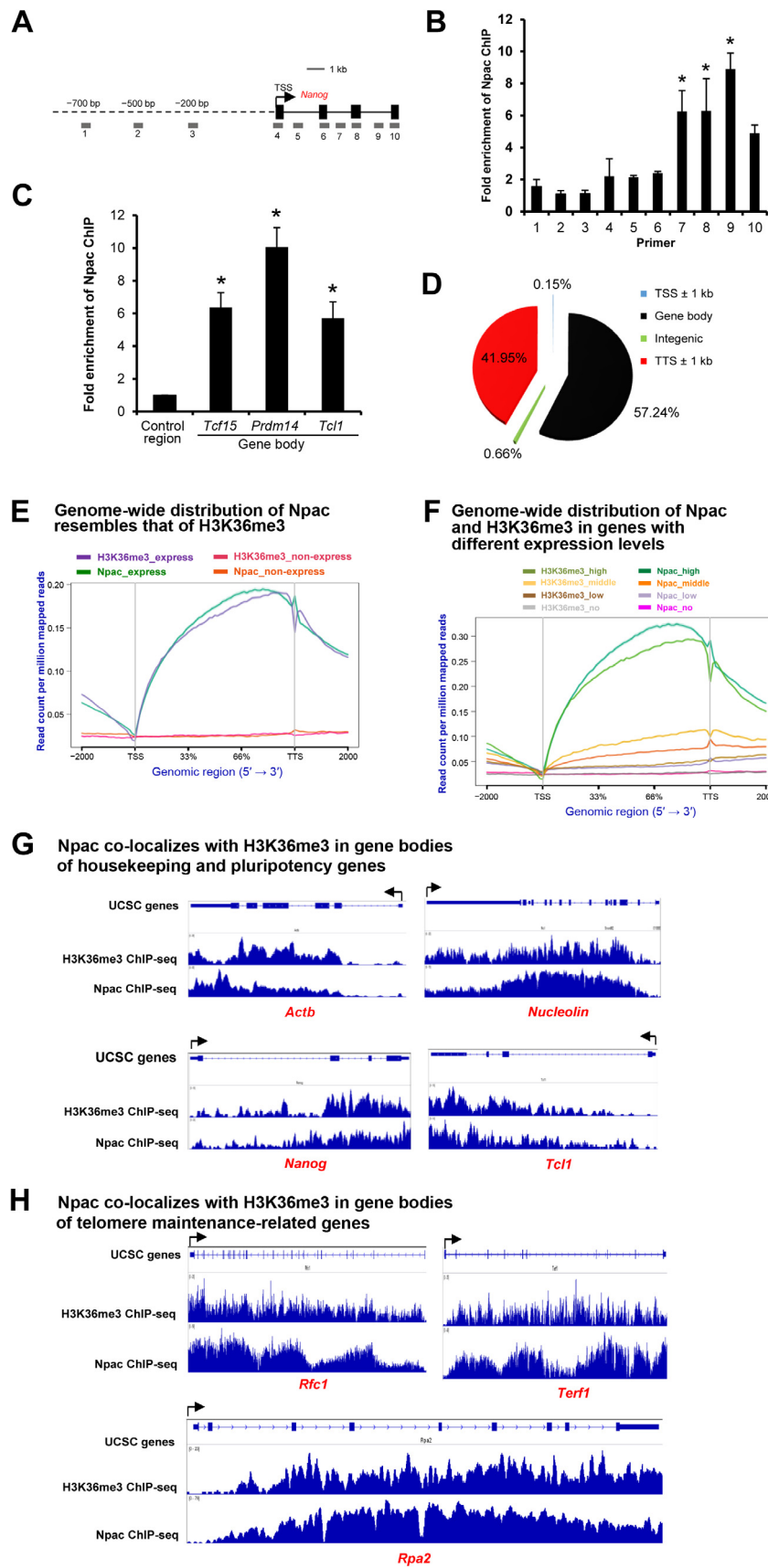


**Figure 4** *Npac* depletion may cause cellular apoptosis

**A.** Heatmap of up-regulated cell death-related genes upon *Npac* KD in mESCs. Genes were selected according to their known functions in cell death. **B.** Cell cycle analysis by flow cytometry in the *Npac* RNAi-1 transfected cells and the control (empty vector) group. **C.** The representative flow cytometry pattern is shown. **D.** Apoptosis triggered by *Npac* KD was analyzed by Annexin V staining through flow cytometry. **E.** Graphical representation of the apoptosis cells detected by Annexin V staining. Data were shown as mean  $\pm$  SE ( $n = 3$ ). \*,  $P < 0.05$  (Student's *t*-test).

respectively (Figure 5D). GO analysis showed that the genes that *Npac* binds to were linked to development, transcription, chromatin modification, cell cycle, and RNA processing (Table S2).

Since *Npac* is a co-factor of LSD2 which demethylates histone H3K4me1 and H3K4me2, we were also interested in the relationship between *Npac* and histone H3K4me2. Indeed, we found that the genome-wide profile of *Npac* localization was



inversely correlated to that of histone H3K4me2 (Figure S5A). We were also keen to explore whether *Npac* is linked to other histone modifications. Here, we chose several important histone modifications (histone H3K9me3, histone H3K27me3, and histone H3K4me3) (Figure S5B) and their respective modifiers (Eset, Ezh2, and MLL2) (Figure S5C), as well as ESC-enriched transcription factors (Oct4, Nanog, and Sox2) (Figure S5D), to compare their distribution patterns with that of *Npac*. We found that *Npac* binding profile displayed a unique pattern compared to the epigenetic modifiers, histone modifications, and ESC-enriched transcription factors we selected. In general, the number of *Npac*-associated genes (most are active genes) is much less than that of other modifiers (Eset, Ezh2, and MLL2). Furthermore, *Npac*, unlike Eset, Ezh2, and MLL2 (mainly located at TSSs), is enriched in gene bodies and 3' ends. Thirdly, *Npac* shares some genomic loci with the master transcription factors Oct/Nanog/Sox2, but the genomic locations of these three transcription factors are different from that of *Npac*.

*Npac* is a putative reader of histone H3K36me3, together with which *Npac* is present almost exclusively over gene bodies [24]. We found that, in mESCs, the genome-wide distribution of *Npac* resembled that of histone H3K36me3: both of *Npac* and H3K36me3 were enriched at active genes in E14 ESCs, where they displayed absence from the TSSs, but gradually increased from gene bodies to TTSs, while they had low or even no binding at inactive genes in E14 ESCs (Figure 5E). We further divided genes into four groups (high, middle, low, and no) according to their expression levels. The results also showed similar genome-wide distribution between *Npac* and H3K36me3, both of which displayed highest binding at genes with high expression, but lower binding at genes with lower expression (Figure 5F). This result further indicated that *Npac* and H3K36me3 were enriched in actively transcribed genes in E14 ESCs. Indeed, we observed that both histone H3K36me3 and *Npac* had high occupancies in actively transcribed genes, such as the housekeeping gene *Actb*, the pluripotency genes *Nanog*, *Nucleolin*, and *Tcl1*, and the telomere maintenance-related genes *Rfc1*, *Terf1*, and *Rpa2* (Figure 5G and H). On the other hand, we observed clearly low *Npac* and histone H3K36me3 occupancies on inactive genes. These genes included developmental genes (Figure S6A), MAPK pathway-related genes (Figure S6B), and cell death-related

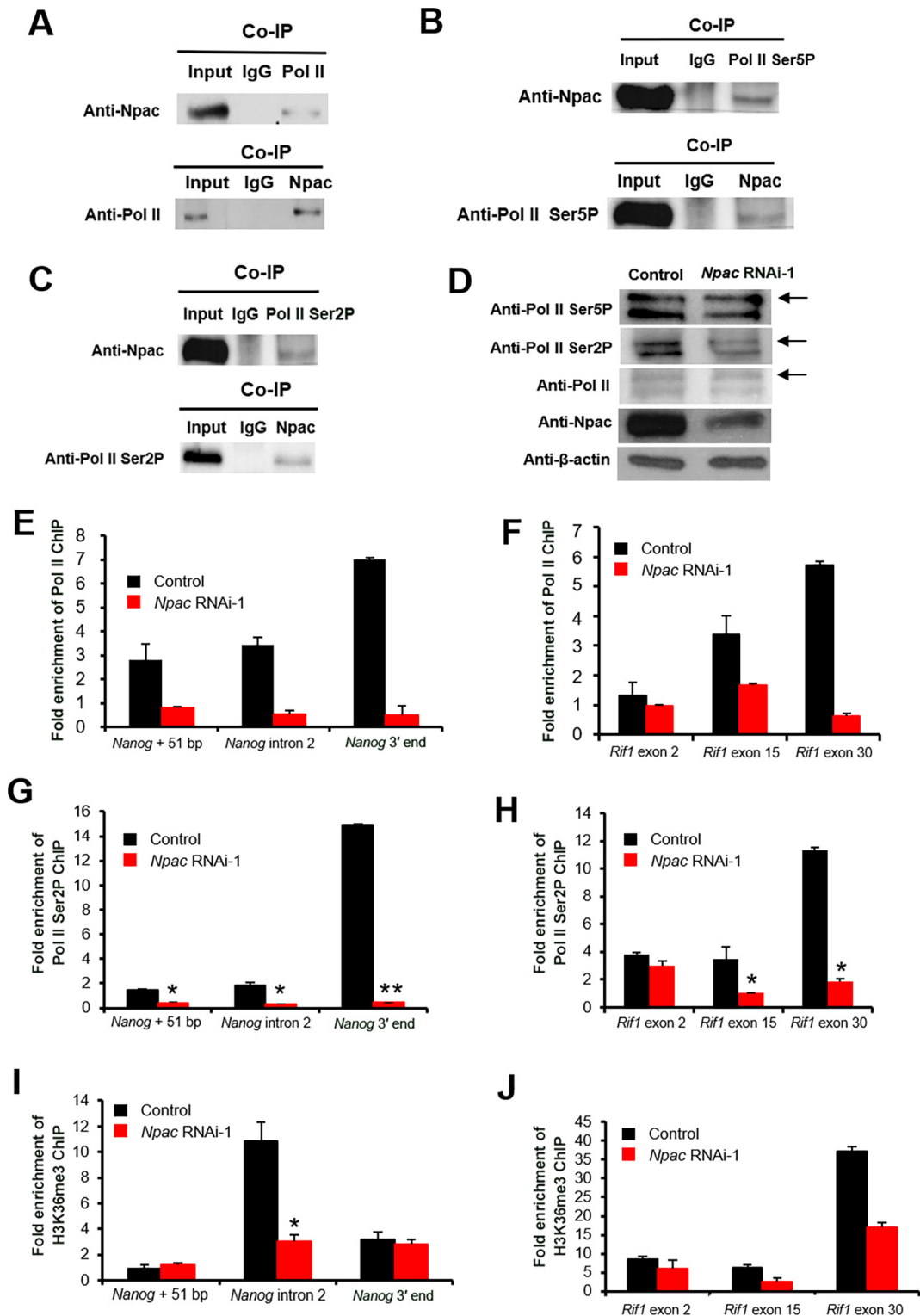
genes (Figure S6C). Taken together, these results show that *Npac* co-localizes with histone H3K36me3 in gene bodies of active genes in mESCs, suggesting that *Npac* plays roles in histone H3K36me3-associated cellular functions including gene activation and transcriptional elongation.

### ***Npac* is likely involved in transcriptional elongation**

Next, we examined how *Npac* is involved in transcriptional elongation. We found that *Npac* can interact with RNA Pol II (Figure 6A). This result is in line with a previous report that the LSD2 complex may include RNA Pol II and *Npac* [28]. We also found that *Npac* can interact with RNA Pol II Ser2P and Ser5P (Figure 6B and C). In addition, we found that the phosphorylation levels of Ser2 and Ser5 were down-regulated upon *Npac* depletion, while RNA Pol II expression was not affected (Figure 6D). This result suggests that the interactions of *Npac* with RNA Pol II Ser2P and Ser5P may affect their phosphorylation levels and functions. Given that Ser5 phosphorylation of RNA Pol II is associated with transcriptional initiation and early elongation while Ser2 phosphorylation correlates with transcriptional elongation [39], we propose that *Npac* affects transcriptional elongation through associating with RNA Pol II Ser2P and Ser5P.

In order to determine whether *Npac* is essential for RNA Pol II-mediated transcriptional elongation in mESCs, we performed ChIP with RNA Pol II, RNA Pol II Ser5P, and RNA Pol II Ser2P in *Npac*-depleted cells and control cells. We performed ChIP-qPCR for the gene bodies of two pluripotency genes *Nanog* and *Rif1*, and *Utrn*, a gene up-regulated in *Npac*-depleted cells. We found that the presence of RNA Pol II and RNA Pol II Ser2P at the gene bodies of *Nanog* (Figure 6E and G) and *Rif1* (Figure 6F and H) was significantly reduced in *Npac*-depleted cells, while their presence at *Utrn* (Figure S7A and B) was not significantly changed. In addition, the level of H3K36me3 was also reduced at the gene bodies of *Nanog* (Figure 6I) and *Rif1* (Figure 6J) in *Npac*-depleted cells. However, the binding of RNA Pol II Ser5P at the gene bodies of *Nanog* (Figure S7C) and *Rif1* (Figure S7D) was similar between the *Npac*-depleted and control cells, suggesting that RNA Pol II Ser5P binding is independent of *Npac*. Taken together, these results suggest that *Npac* promotes transcriptional elongation but does not affect transcriptional initiation.

**Figure 5** *Npac* is mainly located to gene bodies and its genome-wide distribution resembles that of histone H3K36me3  
**A.** Schematic diagram of the structure of the *Nanog* gene. Black boxes represent exons; solid lines represent introns; dashed line represents the promoter; gray boxes at the bottom represent the primers designed at specific areas of the *Nanog* gene. **B.** *Npac* is associated with the *Nanog* gene with high enrichment fold at its gene body. **C.** *Npac* is also associated with the gene bodies of other pluripotency genes including *Tcf15*, *Prdm14*, and *Tcl1*. **D.** Genome-wide distribution of *Npac* in mESCs. **E.** Genome-wide distribution of *Npac* resembles that of histone H3K36me3. H3K36me3\_express and *Npac*\_express represent the genome-wide distributions of H3K36me3 and *Npac* in expressed genes in E14 cells, respectively; H3K36me3\_non-express and *Npac* non-express represent the genome-wide distributions of H3K36me3 and *Npac* in non-expressed genes in E14 cells, respectively. **F.** Genome-wide distributions of *Npac* and H3K36me3 in genes with different expression levels (high, middle, low, and no). H3K36me3\_high/middle/low/no represent the genome-wide distributions of H3K36me3 in genes with high, middle, low, and no expression in mESCs, respectively. *Npac*\_high/middle/low/no represent the genome-wide distributions of *Npac* in genes with high, middle, low, and no expression in mESCs, respectively. Each gene body is represented from 0% (TSS) to 100% (TTS). **G.** *Npac* and H3K36me3 ChIP-seq peaks at the gene bodies of the housekeeping gene (*Actb*) and pluripotency genes (*Nucleolin*, *Nanog*, and *Tcl1*) in mESCs. **H.** *Npac* and H3K36me3 ChIP-seq peaks at the gene bodies of the telomere maintenance-related genes (*Rfc1*, *Terf1*, and *Rpa2*) in mESCs. In (G) and (H), arrows denote TSS and transcription orientation. \*,  $P < 0.05$  (Student's *t*-test). TSS, transcription start site; TTS, transcription termination site.



## **Npac associates with p-TEFb to promote transcriptional elongation**

Next, we observed that *Npac* could interact with p-TEFb, which is composed of Cyclin T1 and Cyclin-dependent kinase 9 (Cdk9) (Figure 7A and B). p-TEFb can phosphorylate the C-terminal domain (CTD) of the large subunit of RNA Pol II, thus promoting transcriptional initiation and elongation [40]. Thus, *Npac* can act as an essential component of the elongation complex. To test whether *Npac* is required for transcriptional elongation, we performed an elongation recovery assay to measure the recovery of transcription at different positions of two genes (*Nanog* and *Rif1*). We first incubated *Npac* RNAi or control (empty vector) transfected cells with 100  $\mu$ M 5,6-dichloro-1- $\beta$ -D-ribofuranosylbenzimidazole (DRB), a widely used elongation inhibitor [41], for 3 h. Then, the cells were washed twice with PBS and cultured with fresh medium without DRB before total RNA was isolated every 5 min (Figure 7C) [37]. We first confirmed that the *Npac* KD efficiency was not affected by the addition of DRB in the *Npac*-depleted cells; about 40% *Npac* mRNA was detected compared to the control group at each time point post DRB treatment (Figure 7D). Next, we examined the transcripts from *Nanog* at different positions (exon 1 and exon 4) after release from the elongation block (Figure 7E). Following the release, the recovery of transcriptional output at exon 4 of *Nanog* was significantly reduced by *Npac* RNAi (Figure 7F), while the recovery of transcriptional output at exon 1 of *Nanog* was not significantly affected (Figure 7G). We next examined the transcripts from *Rif1* at exon 2 and exon 30 after release from elongation block (Figure 7H). Similarly, we observed that the recovery of transcriptional output at exon 2 of *Rif1* was not significantly changed in *Npac*-depleted cells (Figure 7I). However, the recovery of transcriptional output at exon 30 of *Rif1* was largely decreased compared to the control group (Figure 7J). Taken together, these results suggest that *Npac* depletion causes transcriptional elongation defects of *Nanog* and *Rif1*.

## **Discussion**

ESC pluripotency is governed by both genetic and epigenetic mechanisms. Many pluripotency factors including transcription factors and epigenetic regulators have been discovered in ESCs [42]. Our results indicate that *Npac* is required to

maintain pluripotency in mESCs. First, we found that depletion of *Npac* significantly repressed the expression of master pluripotency factors Oct4 and Nanog. Besides these core factors, the expression levels of many other known ESC pluripotency genes also decreased upon *Npac* depletion according to our gene expression microarray. Among these, *Tet1* is specifically expressed in ESCs and required for ESC maintenance [43]. *Tcl1*, encoding a co-factor of the Akt1 kinase, is essential for self-renewal of ESCs [44]. Also, KDM5B, a H3K4me3 demethylase, is an activator of ESC self-renewal correlated genes [45]. Second, transient KD of *Npac* increased the expression of mesoderm and endoderm lineage markers and reduced the AP activity. These results further support the assertion that *Npac* is required for maintaining ESC in an undifferentiated state. Third, we found that *Npac* depletion activated the MAPK/ERK signaling pathway (Figure 3A and D). Previous studies have reported that ERK signaling pathway can induce ESC differentiation into all germ layers *in vitro* [46,47], and activation of ERK represses Nanog expression and causes ESC differentiation into primitive endoderm [48]. Intriguingly, we found that *Npac* depletion led mESCs to differentiation but the ERK inhibitor (PD0325901, Sigma) did not fully rescue the differentiation phenotype. It is noteworthy that ERK inhibitors can block general ESC differentiation and thus may mask true differentiation defects of *Npac*-depleted ESCs. Thus, ERK inhibitors might not be specific to rescue the phenotype resulting from *Npac* depletion. Therefore, though it is possible that reduction of *Nanog* upon *Npac* depletion was partially caused by the activation of ERK pathway, this is unlikely to be the sole mechanism. We surmise that *Npac* depletion also results in changes in chromatin state, RNA binding, and cell metabolism, some of which may be non-reversible. It is highly likely that *Npac* regulates pluripotency using some other unknown mechanisms which will be interesting to be further explored.

Furthermore, the function of *Npac* in somatic reprogramming can also verify its essential role in pluripotency. There are several possible ways in which *Npac* depletion can inhibit the reprogramming process. Reprogramming consists of a set of molecular processes that transform a somatic cell into a pluripotent stem cell. During reprogramming, genes related to differentiated state should be repressed first and markers associated with pluripotency will be activated subsequently. Meanwhile, widespread chromatin remodeling occurs during the whole process [49,50]. Our microarray results showed that *Npac* depletion activates many development-associated genes

## **Figure 6 Npac could be involved in RNA Pol II-mediated transcriptional elongation**

A. *Npac* interacted with RNA Pol II. Cell lysate of wild-type ESCs was immunoprecipitated using either anti-RNA Pol II antibody (upper) or anti-*Npac* antibody (lower). Western blot was subsequently carried out with anti-*Npac* antibody (upper) and anti-RNA Pol II antibody (lower). B. *Npac* can be pulled down with RNA Pol II Ser5P and vice versa. C. *Npac* can be pulled down with RNA Pol II Ser2P and vice versa. D. *Npac* depletion led to down-regulation of RNA Pol II Ser2P and RNA Pol II Ser5P, while total RNA Pol II was not affected.  $\beta$ -actin served as a loading control. Arrows indicate the binds corresponding to RNA Pol II Ser5P, RNA Pol II Ser2P, and RNA Pol II, respectively. E. and F. The binding of RNA Pol II at the gene bodies of *Nanog* (E) and *Rif1* (F) was significantly reduced in *Npac*-depleted cells. G. and H. The binding of RNA Pol II Ser2P at the gene bodies of *Nanog* (G) and *Rif1* (H) was significantly reduced in *Npac*-depleted cells. I. and J. The distributions of H3K36me3 at the gene bodies of *Nanog* (I) and *Rif1* (J) were significantly reduced in *Npac*-depleted cells. In (E), (G), and (I), “*Nanog* + 51 bp” indicates 51 bp downstream region from *Nanog* TSS. \*,  $P < 0.05$  (Student's *t*-test). Co-IP, co-immunoprecipitation; RNA Pol II Ser5P, Ser5-phosphorylated RNA Pol II; RNA Pol II Ser2P, Ser2-phosphorylated RNA Pol II.

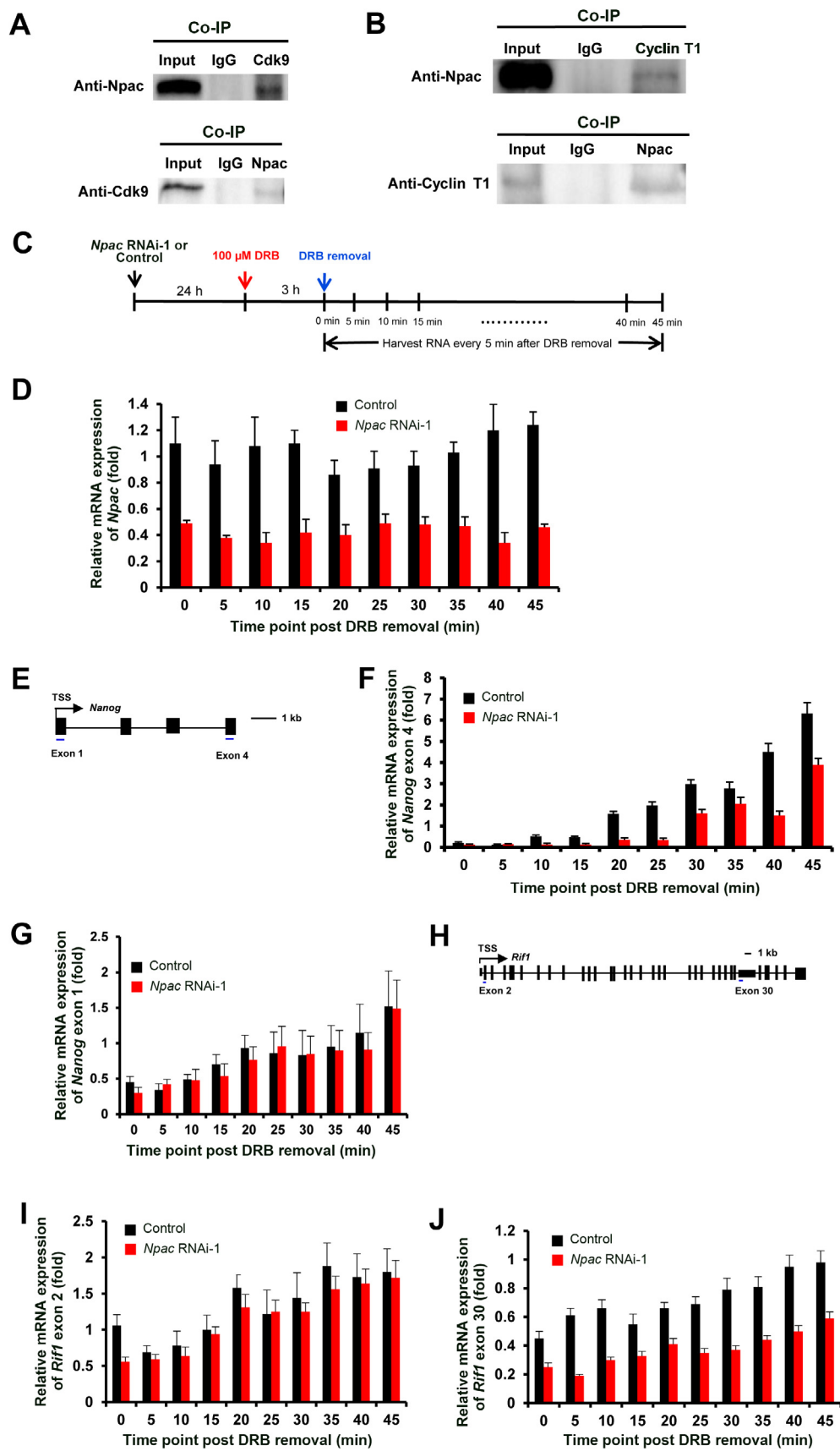


(Figure 3A) and down-regulates a subset of pluripotency genes. Thus, reprogramming may be initially blocked by the high expression of somatic genes upon Npac depletion. It has been demonstrated that active marks, such as H3K4me2/3, can cause chromatin to be in an “open” state and thus enhance iPSC formation, while repressive marks, such as H3K9me and H3K27me, function in the opposite way and impair iPSC formation [50]. Given that H3K36me3 is a mark classically associated with active transcription, we can predict that H3K36me3 marks may promote reprogramming. Thus, the fact that *Npac* KD causes the down-regulation of H3K36me3 (Figure 1C) could be a reason why iPSC formation is inhibited. In addition, GO analysis of microarray and ChIP-seq data revealed that Npac targets many genes that are associated with chromatin modification and nucleosome assembly (Figure 3A). Therefore, this provides additional evidence that Npac depletion may impair reprogramming by inhibiting permissive chromatin state. Finally, the inhibition of the ERK pathway not only enables the maintenance of mESCs in a ground pluripotent state, but can also enhance somatic reprogramming [35,51]. Therefore, the lower reprogramming efficiency of *Npac*-KD MEFs could also be affected by the activation of the ERK pathway.

We found that Npac depletion can increase cellular apoptosis (Figure 4B and D). The mechanisms of apoptosis have been elucidated in numerous studies. Classically, these mechanisms include both extrinsic and intrinsic pathways [52]. Among them, the ERK pathway and p53-dependent apoptosis are two important mechanisms. ERK activity can boost apoptotic pathways by activating Caspase-8 [53]. Thus, the fact that Npac depletion increases the expression of ERK (Figure 3D) and *Caspase-8* (according to our gene expression microarray results) could explain the apoptosis caused by Npac depletion. p53 causes apoptosis by transcription-dependent and -independent mechanisms [54]. Therefore, apoptosis could be induced by affecting p53 downstream targets. Indeed, we observed up-regulated expression of the p53 apoptosis effector related to PMP22 (*Perp*) gene in microarray data (Figure 4A), which is a proapoptotic gene targeted by p53 [55]. Apoptotic protease activating factor-1 (Apaf-1) is another protein up-regulated upon Npac depletion according to our microarray results. Apaf-1 is a component of the apoptotic machinery activated by p53. Because of the unique abbreviated cell cycle, mESCs display a different mechanism of cell cycle arrest and apoptosis compared to somatic cells. Our results showed that Npac-depleted ESCs were arrested in the sub-G1 phase (Figure 4B); this could be another reason why ESCs undergo apoptosis upon Npac depletion. Taken together, our results suggest that Npac depletion causes apoptosis through the p53-dependent pathway and the ERK pathway.

We found that Npac co-localizes with the transcriptional elongation mark histone H3K36me3 in gene bodies of actively transcribed genes in mESCs (Figure 5E and F). This is consistent with the finding from a study in human HeLa cells [24]. However, it remains unclear whether recruitment of Npac depends on the localization of histone H3K36me3. Given that Npac predominantly occupies actively transcribed genes (Figure 5G and H), it appears that Npac functions as a transcriptional activator of these actively transcribed genes (such as the pluripotency genes and telomere maintenance-related genes) in mESCs. Moreover, we observed that the global level of RNA Pol II Ser2P was reduced, while the total RNA Pol II was unaffected when Npac was depleted (Figure 6D). There is a possibility that the lower level of phosphorylated RNA Pol II in Npac-depleted cells reduces the elongation process or even blocks transcriptional elongation. Therefore, most of the active genes in mESCs were down-regulated upon Npac depletion. In addition, the binding of RNA Pol II and RNA Pol II Ser2P at the pluripotency genes *Nanog* and *Rif1* was significantly reduced upon Npac depletion, while the binding of RNA Pol II Ser5P at these two genes did not significantly change. These results further confirmed that Npac is required for transcriptional elongation.

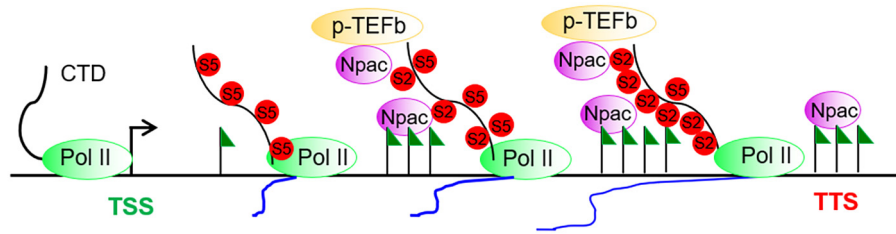
In mammalian cells, Ser2 of RNA Pol II can be phosphorylated by Cdk9 (the kinase subunit of p-TEFb), resulting in the transition from transcriptional initiation to productive elongation [56]. According to previous studies, some specific activators, such as DNA- or RNA-bound activators and co-activators, can recruit p-TEFb to transcription units. For example, one chromatin remodeling protein, Brd4, recruits p-TEFb to stimulate RNA Pol II-dependent transcription [57]. Given the association of Npac with p-TEFb observed in our study (Figure 7A and B), it is possible that Npac recruits p-TEFb to chromatin and further results in the successful transcriptional elongation of target genes. This is in concert with the observation that Npac depletion caused the transcriptional elongation defects of the pluripotency genes *Nanog* and *Rif1*. However, this may not be the sole reason. Lower enrichment of histone H3K36me3 and RNA Pol II Ser2P upon Npac depletion may also contribute to the transcriptional elongation defects. Taken together, these findings imply an essential role of Npac in the elongation process.

Interestingly, according to our Npac gene expression microarray results, we found more up-regulated genes than down-regulated ones upon Npac depletion. This appears to be contrary to the fact that Npac is associated with actively transcribed genes. However, we think that Npac depletion in mESCs results in differentiation and triggers a significant up-regulation of abundant developmental genes which are

## Figure 7 Npac interacts with p-TEFb and Npac depletion may lead to transcriptional elongation defect

A. Npac interacted with Cdk9. B. Npac interacted with Cyclin T1. C. Workflow for the elongation recovery assay. D. *Npac* KD efficiency was not affected by the addition of DRB in Npac-depleted cells. E. Schematic showing the analyzed regions of *Nanog*. F. Changes in the transcription rate of exon 4 of *Nanog* upon Npac depletion. G. Changes in the transcription rate of exon 1 of *Nanog* upon Npac depletion. H. Schematic showing the analyzed regions of *Rif1*. I. Changes in the transcription rate of exon 2 of *Rif1* upon Npac depletion. J. Changes in the transcription rate of exon 30 of *Rif1* upon Npac depletion. In (F), (G), (I), and (J), each graph illustrates the RNA levels at different regions of *Nanog/Rif1* at different recovery time after DRB block was released. Data were shown as mean  $\pm$  SE ( $n = 3$ ). p-TEFb, positive transcriptional elongation factor; Cdk9, Cyclin-dependent kinase 9; DRB, 5,6-dichloro-1- $\beta$ -D-ribofuranosylbenzimidazole.

## A Normal mESCs



## B Npac-depleted mESCs

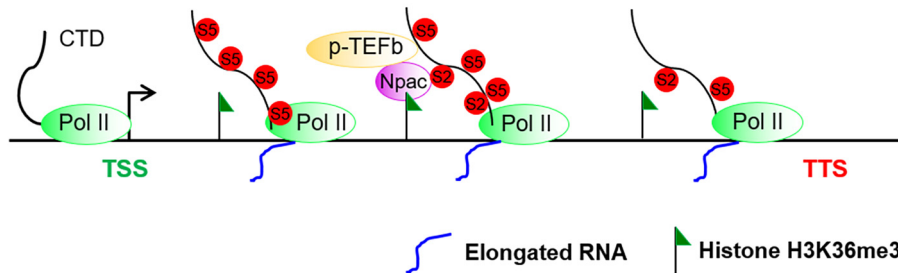


**Figure 8** Model depicting the role of Npac in pluripotency

**A.** In normal mESCs, Npac is expressed at a high level and histone H3K36me3 is enriched in the gene bodies of actively transcribed genes. Npac interacts with RNA Pol II Ser2P and Ser5P and recruits p-TEFb to promote productive elongation. **B.** In Npac-depleted cells, reduction of Npac leads to reduced enrichment of RNA Pol II Ser2P and histone H3K36me3 at the pluripotency genes, thus blocking productive transcriptional elongation. CDT, C-terminal domain.

silenced in undifferentiated mESCs. During the differentiation process, active pluripotency genes become inactivated; meanwhile, silenced developmental genes are activated. Since the activated developmental genes are more than the inactivated pluripotency genes, there are more up-regulated genes than down-regulated genes upon Npac depletion. Furthermore, the activation of the MAPK pathway caused by Npac depletion will trigger many differentiation-related genes. Lastly but not least, the up-regulation of developmental genes in Npac-depleted cells is probably independent of the Npac-mediated transcription elongation, and it could be triggered by ESC differentiation. Nevertheless, given that Npac may have diverse functions, it is of interest to further explore how Npac plays its role in gene regulation during ESC differentiation.

In summary, we propose a model in which Npac regulates mESC pluripotency and influences transcriptional elongation by interacting with p-TEFb, RNA Pol II Ser2P, and RNA Pol II Ser5P (Figure 8A and B).

## Materials and methods

### Cell culture

In this study, mouse E14 ESCs (Catalog No. CRL-1821, ATCC, Manassas, VA), SNL feeder cells (Catalog No. CBA-316, Cell Biolabs, San Diego, CA), Platinum-E cells (Plat-E;

Catalog No. RV-101, Cell Biolabs), and *Oct4-GFP* MEFs were cultured at 37 °C in a CO<sub>2</sub> incubator with 5% CO<sub>2</sub> as previously described [58].

### Construction of plasmids

Plasmids for RNAi-1 and RNAi-2 targeting *Npac* were designed using the Eurofins MWG Operon siMAX software. Oligonucleotides were inserted into the pSuper.puro vector (Catalog No. VEC-pBS-0008, Oligoengine, Seattle, WA). The primers for *Npac* OE were designed by the Primer 5 software to amplify the full-length cDNA of mouse *Npac/Glyr1* (NM\_028720.2), and the PCR product was inserted into the *Bgl*II and *Mlu*I sites of the pPyCAGIP vector. To construct retrovirus packaging plasmids, the full-length *Npac/Glyr1* cDNA was ligated into the *Mlu*I and *Not*I sites of the pMXs plasmid (Catalog No. 18656, Addgene, Watertown, MA). To construct the *Npac* RNAi-resistant plasmid that produces functional Npac protein but is resistant to *Npac* RNAi targeting, specific primers were designed with silent mutations in the sequence of the protein coding domain. The *Npac* RNAi-resistant plasmid was generated according to the manual of Q5 Site-Directed Mutagenesis Kit (Catalog No. E0554S, New England Biolabs, Ipswich, MA). The plasmid with the full-length *Npac* cDNA inserted in the pCAG-Neo vector was used as a PCR template. The sequences of the primers are shown in Table S3.

### Transfection, RNA extraction, reverse transcription, and qRT-PCR

Transfection was conducted using Lipofectamine 2000 (Catalog No. 11668019, Invitrogen, Waltham, MA) according to the manufacturer's protocol. Cells were selected by 1 µg/ml puromycin for 4 days after transfection. Either protein or RNA was then extracted from the cells. RNA extraction, reverse transcription, and qRT-PCR were performed as previously described [58]. The sequences of the qRT-PCR primers are shown in Table S3.

### Gene expression microarray analysis

mESCs (E14) were transfected with *Npac*-KD plasmid or control plasmid and cultured for 4 days with selection. RNA was then extracted from the cells. Gene expression microarray data were analyzed as previously described [58,59].

### ChIP assay and ChIP-seq

ChIP assay and ChIP-seq were conducted as previously described [58,59]. The antibodies used for ChIP were: anti-*Npac* (Catalog No. 14833-1-AP, Proteintech, Rosemont, IL), anti-histone H3K36me3 (Catalog No. ab9050, Abcam, Cambridge, UK), anti-RNA polymerase II CTD repeat YSPTSPS (phospho S2) (Catalog No. ab5095, Abcam), anti-RNA polymerase II CTD repeat YSPTSPS (phospho S5) (Catalog No. ab140509, Abcam).

### Bioinformatics analysis

*Npac* ChIP-seq reads were mapped to the mouse genome (NCBI37/mm9) using the mapping software Burrows-Wheeler Aligner [60]. After removing duplicate reads, the mapped results identified board peaks with MACS2. For location classification, ChIP-seq peaks were annotated by comparing the locations of all TSSs and TTSs in the mouse genome with Perl scripts. (1–10 kb upstream of the TSS defined as upstream, 1 kb upstream of the TSS to the TSS defined as TSS, the region between the TSS and TTS defined as gene body, TTS to 1 kb downstream of the TTS defined as TTS, 1–10 kb downstream of the TTS defined as downstream).

ChIP-seq data of H3K36me3 (ENCSR000CGR), H3K4me3 (GSM1258237) and its modifier MLL2 (GSM1258241), H3K9me3 and its modifier Eset (GSM440256), H3K27me3 (GSM1199184 & GSM1199185) and its modifier EZH2 (GSM1199182 & GSM1199183), Oct4 (GSE65093), Nanog (GSM915363), and Sox2 (GSM1179561) on mouse E14 ESCs were downloaded from ENCODE and compared with the *Npac* ChIP-seq data.

E14 RNA-seq data (GSM1276712) was also downloaded from ENCODE. We used the STAR software [61] to carry out RNA-seq mapping against the mm9 genome. By analyzing the mapped RNA-seq data, featureCounts [62] was used to obtain the gene expression of the E14 sample. All genes were further separated into two groups based on whether the genes were expressed or not. Genes were also classed into four groups based on their expression levels (high, middle, low, and no). Expression levels were classified according to the

number of reads mapped to the mm9 genome. “Reads = 0” represents “non\_express”; “reads > 0” represents “express”; “0 < reads ≤ 10” represents “low expression”; “10 < reads ≤ 100” represents “middle expression”; “reads > 100” represents “high expression”. With the respective gene lists and mapped ChIP-seq files, heatmaps and average read distributions were generated with ngsplot [63].

### Western blot

Western blot was performed as described [58,59]. The primary antibodies used in this study were: anti-*Npac* (Catalog No. 14833-1-AP, Proteintech), anti-NP60 (Catalog No. sc-390601, Santa Cruz, Dallas, TX), anti-β-actin (Catalog No. sc-81178, Santa Cruz), anti-Oct4 (Catalog No. sc-8628, Santa Cruz), anti-Nanog (Catalog No. sc-33760, Santa Cruz), anti-Sox2 (Catalog No. sc-99000, Santa Cruz), anti-p-ERK (Catalog No. 4370, Cell Signaling Technology, Danvers, MA), anti-ERK (Catalog No. 137F5, Cell Signaling Technology), anti-histone H3K36me3 (Catalog No. ab9050, Abcam), anti-Pol II (Catalog No. sc-899, Santa Cruz), anti-RNA polymerase II CTD repeat YSPTSPS (phospho S2) (Catalog No. ab5095, Abcam), anti-RNA polymerase II CTD repeat YSPTSPS (phospho S5) (Catalog No. ab140509, Abcam), anti-Cyclin T1 (Catalog No. sc-10750, Santa Cruz), anti-Cdk9 (Catalog No. sc-484, Santa Cruz), anti-mouse IgG (Catalog No. sc-2025, Santa Cruz), anti-goat IgG (Catalog No. sc-2028, Santa Cruz), and anti-rabbit IgG (Catalog No. sc-2027, Santa Cruz).

### AP staining

AP staining was conducted with the Alkaline Phosphatase Detection Kit (Catalog No. SCR004, Millipore, Burlington, MA) following the manufacturer's protocol. Axio Observer A1 inverted light microscope (Zeiss, Gottingen, Germany) was used to take pictures for the AP staining results.

### Co-immunoprecipitation

Cells were lysed in the lysis buffer (50 mM Tris-HCl pH 8.0, 1 mM EDTA, 150 mM NaCl, 1% NP-40, 10% glycerol) supplemented with a protease inhibitor (Catalog No. 4693159001, Roche, Basel, Switzerland), and rotated for 1 h at 4 °C. After being precleared by protein G beads (Catalog No. 15920010, Invitrogen) for 2 h at 4 °C, the cell lysate was incubated overnight with beads bound by specific antibodies at 4 °C. Then, the beads were washed four times with the lysis buffer and heated in 2× loading dye for 10 min at 95 °C. The supernatant was used for Western blot with specific antibodies. IgG antibody (Catalog No. 12-371, Chemicon, Temecula, CA) was used as the IP control.

### Retrovirus packaging and infection

Retrovirus packaging and infection were carried out as previously described [58]. Briefly, the pMXs retroviral plasmids or pSUPER.retro.puro plasmids were transfected into Plat-E cells. The cells were selected with 1 µg/ml puromycin (Catalog No. P8833, Sigma) and 10 µg/ml blasticidin (Catalog No.

A1113902, Life Technologies, Carlsbad, CA) for 36–48 h. The retroviruses were harvested and concentrated with centrifugal filter units (Catalog No. C7715, Millipore). *Pou5f1-GFP* MEFs were seeded into 24-well plates for 6 h and then infected with retroviruses. Infected MEFs were seeded onto SNL feeder layers 2 days after infection and cultured with mESC medium without LIF until day 5 after infection. The MEFs were then cultured with KSR medium from day 6 after infection. The number of GFP<sup>+</sup> colonies was recorded daily until day 14 after infection. AP staining assays were also conducted at day 14.

#### Annexin V-FITC apoptosis assay

Annexin V-FITC apoptosis assay was carried out as described in the manufacturer's protocol (APOAF, Sigma). After transfected with the *Npac* RNAi or control (empty vector) plasmid in 6-well dishes and selected for 4 days, the cells were stained with Annexin V-FITC and propidium iodide. The cells were then analyzed by flow cytometer (BD FACSCanto, BD Biosciences, San Jose, CA).

#### Cell cycle analysis

Cell cycle analysis was conducted as previously described [58]. Briefly, mESCs were transfected with the *Npac* RNAi plasmid or the control plasmid and selected with puromycin for 4 days. Then, the cells were stained with 50 µg/ml propidium iodide and analyzed by the flow cytometer (BD FACSCanto, BD Biosciences) using Flowing Software 2.5.0.

#### Transcription elongation assay

Transcriptional elongation assay was carried out as previously described [64,65]. E14 cells were transfected with *Npac* RNAi-1 or control (empty vector). After 24 h, the cells were treated with 100 µM DRB (Catalog No. 287891, Sigma) for 3 h, washed twice with PBS, and cultured in fresh medium for different durations (5–45 min). Total RNA was extracted, and qRT-PCR was performed to quantify the changes in the relative expression levels of different regions along the *Rif1* and *Nanog* genes. Gene expression levels were normalized against the expression level of *Actb*. The sequences of used primers are listed in Table S3.

#### Statistical analysis

All experiments were conducted in triplicates. Student's *t*-test was applied for statistical analysis, and the results were shown as mean ± SE.  $P < 0.05$  was considered significant (\*,  $P < 0.05$ ; \*\*,  $P < 0.01$ ; \*\*\*,  $P < 0.001$ ).

#### Data availability

The *Npac* RNAi microarray results and *Npac* ChIP-seq results have been deposited in the NCBI Gene Expression Omnibus (GEO: GSE93296 and GSE95671, respectively), which are publicly accessible at <https://www.ncbi.nlm.nih.gov/geo>. The results have also been deposited in the Genome Sequence

Archive [66] at the National Genomics Data Center, Beijing Institute of Genomics, Chinese Academy Sciences / China National Center for Bioinformation (GSA: CRA003053), which are publicly accessible at <https://ngdc.cncb.ac.cn/gsa>.

#### CRediT author statement

**Sue Yu:** Conceptualization, Methodology, Data curation, Writing - original draft. **Jia Li:** Methodology, Data curation, Software. **Guanxu Ji:** Data curation. **Zhen Long Ng:** Data curation. **Jiamin Siew:** Data curation. **Wan Ning Lo:** Data curation. **Ying Ye:** Methodology. **Yuan Yuan Chew:** Validation. **Yun Chau Long:** Resources, Supervision. **Wensheng Zhang:** Methodology. **Ernesto Guccione:** Funding acquisition. **Yuin Han Loh:** Funding acquisition. **Zhi-Hong Jiang:** Resources, Supervision, Project administration. **Henry Yang:** Conceptualization, Methodology, Software. **Qiang Wu:** Conceptualization, Methodology, Formal analysis, Investigation, Data curation, Writing - original draft, Writing - review & editing, Visualization. All authors have read and approved the final manuscript.

#### Competing interests

The authors have declared that no competing interests exist.

#### Acknowledgments

We thank Dr. Takao Inoue for critical reading of the manuscript. We thank Prof. Huck Hui Ng for providing *Oct4-GFP* MEFs. This work was supported by Singapore National Medical Research Council (Grant No. CBRG14nov065) and the Macau Science and Technology Development Fund, China (Grant No. FDCT-18-033-SKL-016A).

#### Supplementary material

Supplementary data to this article can be found online at <https://doi.org/10.1016/j.gpb.2020.08.004>.

#### ORCID

ORCID 0000-0003-1838-6506 (Sue Yu)  
 ORCID 0000-0001-8360-3912 (Jia Li)  
 ORCID 0000-0002-0384-2890 (Guanxu Ji)  
 ORCID 0000-0001-8154-447X (Zhen Long Ng)  
 ORCID 0000-0001-7968-2742 (Jiamin Siew)  
 ORCID 0000-0001-8778-0457 (Wan Ning Lo)  
 ORCID 0000-0002-5028-3112 (Ying Ye)  
 ORCID 0000-0002-6116-5330 (Yuan Yuan Chew)  
 ORCID 0000-0001-5692-0381 (Yun Chau Long)  
 ORCID 0000-0002-6876-3173 (Wensheng Zhang)  
 ORCID 0000-0001-7764-5307 (Ernesto Guccione)  
 ORCID 0000-0002-4715-6454 (Yuin Han Loh)  
 ORCID 0000-0002-7956-2481 (Zhi-Hong Jiang)  
 ORCID 0000-0002-1155-8216 (Henry Yang)  
 ORCID 0000-0003-2049-1639 (Qiang Wu)

## References

- [1] Evans MJ, Kaufman MH. Establishment in culture of pluripotential cells from mouse embryos. *Nature* 1981;292:154–6.
- [2] Martin GR. Isolation of a pluripotent cell line from early mouse embryos cultured in medium conditioned by teratocarcinoma stem cells. *Proc Natl Acad Sci U S A* 1981;78:7634–8.
- [3] Keller G. Embryonic stem cell differentiation: emergence of a new era in biology and medicine. *Genes Dev* 2005;19:1129–55.
- [4] Smith A. Cell therapy: in search of pluripotency. *Curr Biol* 1998;8:802–4.
- [5] Vitale AM, Wolvetang E, Mackay-Sim A. Induced pluripotent stem cells: a new technology to study human diseases. *Int J Biochem Cell Biol* 2011;43:843–6.
- [6] Amabile G, Meissner A. Induced pluripotent stem cells: current progress and potential for regenerative medicine. *Trends Mol Med* 2009;15:59–68.
- [7] Takahashi K, Yamanaka S. Induction of pluripotent stem cells from mouse embryonic and adult fibroblast cultures by defined factors. *Cell* 2006;126:663–76.
- [8] Yu J, Vodyanik MA, Smuga-Otto K, Antosiewicz-Bourget J, Frane JL, Tian S, et al. Induced pluripotent stem cell lines derived from human somatic cells. *Science* 2007;318:1917–20.
- [9] Nichols J, Zevnik B, Anastasiadis K, Niwa H, Klewe-Nebenius D, Chambers I, et al. Formation of pluripotent stem cells in the mammalian embryo depends on the POU transcription factor Oct4. *Cell* 1998;95:379–91.
- [10] Avilion AA, Nicolis SK, Pevny LH, Perez L, Vivian N, Lovell-Badge R. Multipotent cell lineages in early mouse development depend on SOX2 function. *Genes Dev* 2003;17:126–40.
- [11] Chambers I, Colby D, Robertson M, Nichols J, Lee S, Tweedie S, et al. Functional expression cloning of Nanog, a pluripotency sustaining factor in embryonic stem cells. *Cell* 2003;113:643–55.
- [12] Mitsui K, Tokuzawa Y, Itoh H, Segawa K, Murakami M, Takahashi K, et al. The homeoprotein Nanog is required for maintenance of pluripotency in mouse epiblast and ES cells. *Cell* 2003;113:631–42.
- [13] Young RA. Control of the embryonic stem cell state. *Cell* 2011;144:940–54.
- [14] Jaenisch R, Young R. Stem cells, the molecular circuitry of pluripotency and nuclear reprogramming. *Cell* 2008;132:567–82.
- [15] Yeo JC, Ng HH. The transcriptional regulation of pluripotency. *Cell Res* 2013;23:20–32.
- [16] De Los Angeles A, Ferrari F, Xi R, Fujiwara Y, Benvenisty N, Deng H, et al. Hallmarks of pluripotency. *Nature* 2015;525:469–78.
- [17] Mattout A, Meshorer E. Chromatin plasticity and genome organization in pluripotent embryonic stem cells. *Curr Opin Chem Biol* 2010;22:334–41.
- [18] Efroni S, Duttagupta R, Cheng J, Dehghani H, Hoepfner DJ, Dash C, et al. Global transcription in pluripotent embryonic stem cells. *Cell Stem Cell* 2008;2:437–47.
- [19] Ringrose L, Paro R. Epigenetic regulation of cellular memory by the Polycomb and Trithorax group proteins. *Annu Rev Genet* 2004;38:413–43.
- [20] Mikkelsen TS, Ku M, Jaffe DB, Issac B, Lieberman E, Giannoukos G, et al. Genome-wide maps of chromatin state in pluripotent and lineage-committed cells. *Nature* 2007;448:553–60.
- [21] Brien GL, Gambero G, O'Connell DJ, Jerman E, Turner SA, Egan CM, et al. Polycomb PHF19 binds H3K36me3 and recruits PRC2 and demethylase NO66 to embryonic stem cell genes during differentiation. *Nat Struct Mol Biol* 2012;19:1273–81.
- [22] Zhang Y, Xie S, Zhou Y, Xie Y, Liu P, Sun M, et al. H3K36 histone methyltransferase Setd2 is required for murine embryonic stem cell differentiation toward endoderm. *Cell Rep* 2014;8:1989–2002.
- [23] Kolasinska-Zwier P, Down T, Latorre I, Liu T, Liu XS, Ahringer J. Differential chromatin marking of introns and expressed exons by H3K36me3. *Nat Genet* 2009;41:376–81.
- [24] Vermeulen M, Eberl HC, Matarese F, Marks H, Denissov S, Butter F, et al. Quantitative interaction proteomics and genome-wide profiling of epigenetic histone marks and their readers. *Cell* 2010;142:967–80.
- [25] Vezzoli A, Bonadies N, Allen MD, Freund SM, Santiveri CM, Kvinlaug BT, et al. Molecular basis of histone H3K36me3 recognition by the PWWP domain of Brpf1. *Nat Struct Mol Biol* 2010;17:617–9.
- [26] Wu H, Zeng H, Lam R, Tempel W, Amaya MF, Xu C, et al. Structural and histone binding ability characterizations of human PWWP domains. *PLoS One* 2011;6:e18919.
- [27] van Nuland R, van Schaik FMA, Simonis M, van Heesch S, Cuppen E, Boelens R, et al. Nucleosomal DNA binding drives the recognition of H3K36-methylated nucleosomes by the PSIP1-PWWP domain. *Epigenetics Chromatin* 2013;6:12.
- [28] Fang R, Barbera A, Xu Y, Rutenberg M, Leonor T, Bi Q, et al. Human LSD2/KDM1b/AOF1 regulates gene transcription by modulating intragenic H3K4me2 methylation. *Mol Cell* 2010;39:222–33.
- [29] Fang R, Chen F, Dong Z, Hu D, Barbera AJ, Clark EA, et al. LSD2/KDM1B and its cofactor NPAC/GLYR1 endow a structural and molecular model for regulation of H3K4 demethylation. *Mol Cell* 2013;49:558–70.
- [30] Marabelli C, Marrocco B, Pilotto S, Chittori S, Picaud S, Marchese S, et al. Tail-based mechanism drives nucleosome demethylation by the LSD2/NPAC multimeric complex. *Cell Rep* 2019;27:387–99.
- [31] Niwa H, Miyazaki J, Smith AG. Quantitative expression of Oct-3/4 defines differentiation, dedifferentiation or self-renewal of ES cells. *Nat Genet* 2000;24:372–6.
- [32] Leahy A, Xiong JW, Kuhert F, Stuhlmann H. Use of developmental marker genes to define temporal and spatial patterns of differentiation during embryoid body formation. *J Exp Zool* 1999;284:67–81.
- [33] Kim JB, Zaehres H, Wu G, Gentile L, Ko K, Sebastiano V, et al. Pluripotent stem cells induced from adult neural stem cells by reprogramming with two factors. *Nature* 2008;454:646–50.
- [34] Ying QL, Wray J, Nichols J, Batlle-Morera L, Doble B, Woodgett J, et al. The ground state of embryonic stem cell self-renewal. *Nature* 2008;453:519–23.
- [35] Nichols J, Silva J, Roode M, Smith A. Suppression of Erk signalling promotes ground state pluripotency in the mouse embryo. *Development* 2009;136:3215–22.
- [36] Yang SH, Kalkan T, Morrisroe C, Smith A, Sharrocks AD. A genome-wide RNAi screen reveals MAP kinase phosphatases as key ERK pathway regulators during embryonic stem cell differentiation. *PLoS Genet* 2012;8:e1003112.
- [37] Luo Y, Lim CL, Nichols J, Martinez-Arias A, Wernisch L. Cell signalling regulates dynamics of Nanog distribution in embryonic stem cell populations. *J R Soc Interface* 2013;10:20120525.
- [38] Hamilton WB, Kaji K, Kunath T. ERK2 suppresses self-renewal capacity of embryonic stem cells, but is not required for multi-lineage commitment. *PLoS One* 2013;8:e60907.
- [39] Sims RJ, Belotserkovskaya R, Reinberg D. Elongation by RNA polymerase II: the short and long of it. *Genes Dev* 2004;18:2437–68.
- [40] Price DH. P-TEFb, a cyclin-dependent kinase controlling elongation by RNA polymerase II. *Mol Cell Biol* 2000;20:2629–34.
- [41] Bensaude O. Inhibiting eukaryotic transcription. Which compound to choose? How to evaluate its activity? *Transcription* 2011;2:103–8.
- [42] Liu N, Lu M, Tian X, Han Z. Molecular mechanisms involved in self-renewal and pluripotency of embryonic stem cells. *J Cell Physiol* 2007;211:279–86.

- [43] Ito S, D'Alessio AC, Taranova OV, Hong K, Sowers LC, Zhang Y. Role of Tet proteins in 5mC to 5hmC conversion, ES-cell self-renewal and inner cell mass specification. *Nature* 2010;466:1129–33.
- [44] Ivanova N, Dobrin R, Lu R, Kotenko I, Levorse J, DeCoste C, et al. Dissecting self-renewal in stem cells with RNA interference. *Nature* 2006;442:533–8.
- [45] Xie L, Pelz C, Wang W, Bashar A, Varlamova O, Shadle S, et al. KDM5B regulates embryonic stem cell self-renewal and represses cryptic intragenic transcription. *EMBO J* 2011;30:1473–84.
- [46] Kunath T, Saba-El-Leil MK, Almousaillekh M, Wray J, Meloche S, Smith A. FGF stimulation of the Erk1/2 signalling cascade triggers transition of pluripotent embryonic stem cells from self-renewal to lineage commitment. *Development* 2007;134:2895–902.
- [47] Hamilton WB, Brickman JM. Erk signaling suppresses embryonic stem cell self-renewal to specify endoderm. *Cell Rep* 2014;9:2056–70.
- [48] Hamazaki T, Kehoe SM, Nakano T, Terada N. The Grb2/Mek pathway represses Nanog in murine embryonic stem cells. *Mol Cell Biol* 2006;26:7539–49.
- [49] Brambrink T, Foreman R, Welstead GG, Lengner CJ, Wernig M, Suh H, et al. Sequential expression of pluripotency markers during direct reprogramming of mouse somatic cells. *Cell Stem Cell* 2008;2:151–9.
- [50] Apostolou E, Hochedlinger K. Chromatin dynamics during cellular reprogramming. *Nature* 2013;502:462–71.
- [51] Lin T, Ambasudhan R, Yuan X, Li W, Hilcove S, Abujarour R, et al. A chemical platform for improved induction of human iPS cells. *Nat Methods* 2009;6:805–8.
- [52] Elmore S. Apoptosis: a review of programmed cell death. *Toxicol Pathol* 2007;35:495–516.
- [53] Cagnol S, Chambard JC. ERK and cell death: mechanisms of ERK-induced cell death – apoptosis, autophagy and senescence. *FEBS J* 2010;277:2–21.
- [54] Fridman JS, Lowe SW. Control of apoptosis by p53. *Oncogene* 2003;22:9030–40.
- [55] Attardi LD, Reczek EE, Cosmas C, Demicco EG, McCurrach ME, Lowe SW, et al. PERP, an apoptosis-associated target of p53, is a novel member of the PMP-22/gas3 family. *Genes Dev* 2000;14:704–18.
- [56] Peterlin BM, Price DH. Controlling the elongation phase of transcription with P-TEFb. *Mol Cell* 2006;23:297–305.
- [57] Jang MK, Mochizuki K, Zhou M, Jeong HS, Brady JN, Ozato K. The bromodomain protein Brd4 is a positive regulatory component of P-TEFb and stimulates RNA polymerase II-dependent transcription. *Mol Cell* 2005;19:523–34.
- [58] Yu S, Ma H, Ow JR, Goh Z, Chiang R, Yang H, et al. Zfp553 is essential for maintenance and acquisition of pluripotency. *Stem Cells Dev* 2016;25:55–67.
- [59] Ma H, Ng HM, Teh X, Li H, Lee YH, Chong YM, et al. Zfp322a regulates mouse ES cell pluripotency and enhances reprogramming efficiency. *PLoS Genet* 2014;10:e1004038.
- [60] Li H. Toward better understanding of artifacts in variant calling from high-coverage samples. *Bioinformatics* 2014;30:2843–51.
- [61] Dobin A, Davis CA, Schlesinger F, Drenkow J, Zaleski C, Jha S, et al. STAR: ultrafast universal RNA-seq aligner. *Bioinformatics* 2013;29:15–21.
- [62] Liao Y, Smyth GK, Shi W. featureCounts: an efficient general purpose program for assigning sequence reads to genomic features. *Bioinformatics* 2014;30:923–30.
- [63] Shen L, Shao N, Liu X, Nestler E. ngs.plot: quick mining and visualization of next-generation sequencing data by integrating genomic databases. *BMC Genomics* 2014;15:284.
- [64] Singh J, Padgett RA. Rates of *in situ* transcription and splicing in large human genes. *Nat Struct Mol Biol* 2009;16:1128–33.
- [65] Lemieux B, Blanchette M, Monette A, Mouland AJ, Wellinger RJ, Chabot B. A function for the hnRNP A1/A2 proteins in transcription elongation. *PLoS One* 2015;10:e0126654.
- [66] Chen T, Chen X, Zhang S, Zhu J, Tang B, Wang A, et al. The Genome Sequence Archive Family: toward explosive data growth and diverse data types. *Genomics Proteomics Bioinformatics* 2021;19:578–83.